Progress In Electromagnetics Research M, Vol. 54, 183–193, 2017

Investigation of an Electrically Small Half-Loop Antenna Embedded with a Non-Foster Network Using the Characteristic Mode Theory

Li Sun*, Bao-Hua Sun, and Guan-Xi Zhang

Abstract—An electrically small half-loop antenna (ESHLA) embedded with Foster elements is analyzed using the characteristic mode (CM) theory. The resonant frequency and radiation characteristics of the ESHLA are mainly determined by the resonant mode (Mode 1). The characteristic currents of resonant mode (Mode 1) and non-resonant mode (higher order mode) prove the parallel resonance of the ESHLA. However, owing to the modal significance (MS) of the resonant mode varying fast with frequency, the proposed ESHLA has a narrow bandwidth. Analysis shows the MS of the resonant mode and the higher order mode are changed by tuning the Foster element, leading to a negative admittance variation slope in accordance with the non-Foster behavior. By replacing the Foster capacitor with the non-Foster network, both the characteristic currents and the MS are changed over a wide bandwidth. As a consequence, the introduced non-Foster network turns Mode 1 from the narrowband resonant mode into a continuous resonant mode with its radiation pattern kept invariant over a wide bandwidth. The proposed ESHLA with its non-Foster network is fabricated and measured. The measured 6-dB return loss bandwidth is about 12.7% (11.45–13 MHz), with its reflection coefficient curve being an envelope of those of Foster elements embedded ESHLA.

1. INTRODUCTION

High frequency (HF; 3–30 MHz) band antennas have been widely used in vehicle-antenna systems for medium and long distance communication. In traditional vehicle-antenna systems, vertical whip antennas, horizontal dipole antennas, and loop antennas are conventional choices to establish mobile communications at HF band [1]. A horizontal dipole launches skywave, which limits the frequency band between 2 and 12 MHz. Due to the huge size, it is difficult for horizontal dipole to suit for mobile platform [2]. Frequently, the vertical whip antenna mounted vertically on a mobile platform becomes one of the standard mobile-antenna configurations. Unfortunately, such an orientation produces almost no radiation in the required direction. To solve this problem, tilting the whip is a good method to enhance its radiation toward the zenith. However, this can degrade other characteristics of the antenna, such as radiation efficiency. Under condition of the same size with the whip antenna, the HF band vehicle-mounted loop antenna has not only lower elevation but also higher efficiency. Half-loop antenna is a mobile configuration with a half-circle or half-rectangle of wire mounted perpendicularly on a conducting plane. Being considered as a magnetic dipole, electrically small half-loop antenna (ESHLA) has the ability to conduct a quasi-constant current. However, the ESHLA itself has the characteristics of low radiation resistance and high reactance, leading to poor radiation efficiency and high non-propagating energy. Using impedance matching techniques, the reactive component can be cancelled over a narrow bandwidth.

Received 4 January 2017, Accepted 3 February 2017, Scheduled 22 February 2017

* Corresponding author: Li Sun (sunli574962432@163.com).

The authors are with the National Laboratory of Science and Technology on Antennas and Microwaves, Xidian University, Xi'an, Shaanxi 710071, China.

Various ESHLAs have been studied over the past few years. The detailed electromagnetic analysis about half-loop antenna [3, 4] or the multi-turn half-loop antenna [5] dates back to the 1990s. One typical way to resonate the ESHLA is capacitive loading [6–8]. By introducing the lumped capacitance and inductance, the antenna in [6] works at 434 MHz ISM (Industrial Scientific Medical) band with the size of 18 mm × 18 mm × 12 mm in the sensor package. By tuning a series of switchable capacitors that are parallel with the antenna [7, 8], the ESHLA resonance is shifted from 2 to 12 MHz, with each frequency band of 3.5 kHz. However, the bandwidths of all these antennas are narrow. It is restricted to the fundamental limit of electrically small antennas described by Wheeler and Chu [9, 10], that passive impedance matching networks provide limited bandwidth improvement. Split ring resonators (SRR) are a valid method to shift down the resonant frequency of a half-loop antenna [11–13]. By placing an optimized SRR adjacent to a loop antenna, the resonant frequency of the antenna shifts from 2.45 GHz to 960 MHz [11]. However, the added SRR structure increases the size of the whole antenna which must be taken into account.

Owing to these critical issues in traditional ESHLA, it is desirable for antennas in the future generations to be wideband, low profile, and compact. Using a non-Foster matching network might be a promising solution. Non-Foster circuits violate the Foster's reactance theorem because they produce a reactance that has a negative slope with frequency. Thus, they can overcome the gain-bandwidth restriction and provide a significant improvement in power efficiency. Recently, non-Foster circuits have been integrated with antennas to achieve active matching [14–18]. A microstrip slotted monopole antenna [14], a parasitic SRR [15], and small loop antennas [16–18] are all loaded with non-foster elements successfully to compensate the antenna reactance and achieve broadband matching.

In this paper, an ESHLA embedded with Foster elements is investigated using the characteristic mode (CM) theory [19–21]. Compared to conventional full-wave electromagnetic analysis, the CM theory has the advantage of visually providing the in-depth physical insight of the radiating phenomena of the proposed antenna structure [22–26]. Analysis shows that the sharp variation of the modal significance (MS) of the resonant mode leads to a limited bandwidth and frequency dependent radiation pattern. By introducing the non-Foster network replacing the Foster capacitor embedded at the end of the ESHLA, the narrowband resonant mode changes into a continuous resonant mode, with its radiation pattern kept invariant over a wide bandwidth.

2. ANTENNA DESIGN AND CHARACTERISTIC MODES ANALYSIS

2.1. Antenna Design

We employ the CM theory to study the resonance and radiation characteristics of the ESHLA in this section. As shown in Fig. 1, the ESHLA consists of a rectangular half-loop, an inverted L-shaped feeding structure, an inductor and a capacitor. The half-loop and the feeding structure are made by copper with diameters of $D1$ and $D2$, respectively. The feeding structure serves as an impedance transformer for matching purpose. A 50 Ω feeding probe is connected to the bottom of the feeding structure. The ground plane in the simulation is treated as a 4.8 m × 3.6 m copper with a height of 3 mm to simulate the plane on a vehicle. Two split parts of the rectangular half-loop are connected with the lumped inductor. An $L = 1\,\mu$H inductor is selected as the base design. A miniaturized design could be achieved with the inductor. Meanwhile, selecting different inductor values makes the half-loop antenna design more compact and tunable. The lumped element capacitor is embedded between the end of the rectangular half-loop and the ground plane. By tuning the value of the capacitor, the resonant frequency varies regularly. In our design, the initial value of the capacitor is $C = 2$ pF. The whole structure is placed perpendicular in the middle of the ground, with a total size of 1.2 m × 0.6 m ($0.05\lambda \times 0.025\lambda$, where λ is the free-space wavelength at 15 MHz). The detailed dimensions of the antenna are listed in Table 1. The calculated reflection coefficient in Fig. 2 shows that the proposed ESHLA only resonates weakly at 13.45 MHz. Besides, the imaginary and the real parts of the input impedance, as shown in Fig. 2, indicate that a parallel resonance occurs at 13.45 MHz.

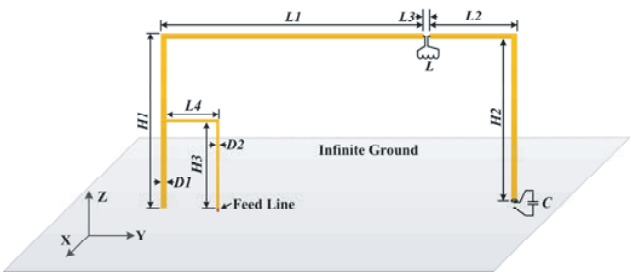

Figure 1. Geometry of electrically small half loop antenna.

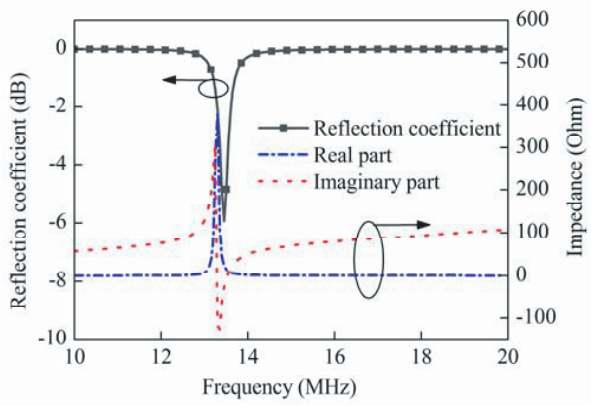

Figure 2. The impedance and reflection coefficient against frequency for the ESHLA embedded with Foster elements.

Table 1. Detailed dimensions of the proposed antenna.

Parameters	$L1$	$L2$	$L3$	$L4$	$H1$	$H2$	$H3$	$D1$	$D2$
Values/m	1.79	0.6	0.01	0.2	1.2	1.19	0.6	0.08	0.02

2.2. CM Analysis

Analyzing the CM of the ESHLA conveniently, the simulated results are obtained using the commercial software FEKO 7.0. The resonant characteristic of the antenna is confirmed by obtaining the MS results as shown in Fig. 3. From Fig. 3, it clearly shows that Mode 1 is a narrowband resonant mode, which has a peak value of MS close to unity at 13.5 MHz. The MS of the other modes increase with frequency. It is readily seen that Mode 3 and Mode 4 contribute very little radiated energy around 13.45 MHz for any external excitation because their associated MS results (< 0.1) clearly indicate the difficulty to excite them. Combining the reflection coefficient result of the antenna, it is found that the resonant frequency

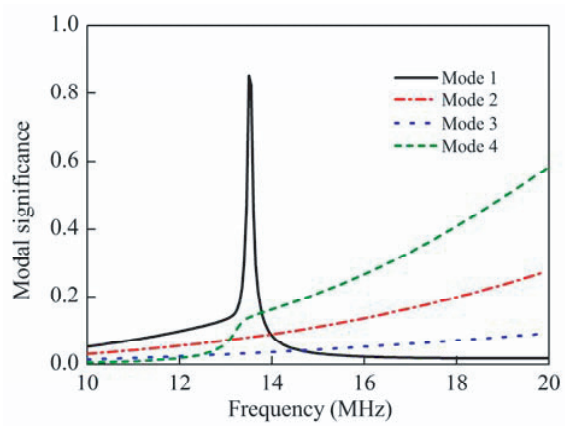

Figure 3. The model significance against frequency for the ESHLA embedded with Foster elements.

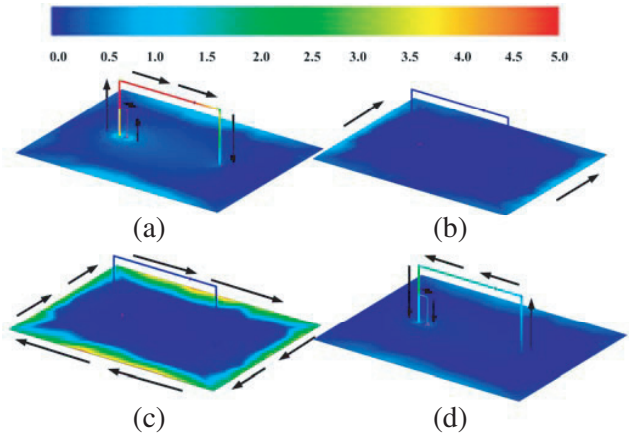

Figure 4. Characteristic currents of the first four modes at 13.45 MHz for ESHLA embedded with Foster elements. (a) Mode 1, (b) Mode 2, (c) Mode 3, and (d) Mode 4.

is not located at the peak of the MS of Mode 1. It implies that other higher order modes participate in the resonance. Because the MS of Mode 4 increases quickly around resonant frequency while slowly over the rest frequency band, we can conclude that both Mode 1 and Mode 4 influence the resonant characteristic of the proposed antenna. To further investigate the resonant behavior of the antenna, we exhibit the characteristic currents of the first four modes at 13.45 MHz in Fig. 4. The black arrows indicate the direction of the currents. Results show that the characteristic currents of Mode 1 and Mode 4 are largely focused on the half-loop, whereas those of Mode 3 are concentrated on the edge of the finite ground. Mode 2 almost does not participate in the resonance. What's more, the flow directions on the antenna of Mode 1 and Mode 4 are opposite. Therefore, both Mode 1 and Mode 4 participate in the resonance, where Mode 1 is the resonant mode. The opposite current directions of Mode 1 and Mode 4 result in a parallel resonance of the antenna.

3. PARAMETER STUDY ON FOSTER ELEMENTS AND DETERMINATION OF NON-FOSTER NETWORK

Once the size of the ESHLA is determined, the resonant frequency can be tuned by changing the Foster elements embedded in the antenna. The proposed antenna operates at parallel resonance, and tuning both inductor and capacitor can change the resonant frequency. Compared to the inductor, tuning the capacitor causes a more obvious and regular change of the resonant frequency. Thus, we just analyze how the Foster capacitor influences the CMs. Because both Mode 1 and Mode 4 influence the resonance of the ESHLA, we focus on the variations of the MS of Mode 1 and Mode 4 with the tuning capacitors. Therefore, we can figure out the method to eliminate the sharp variations of the MS with frequency, achieving a broadband antenna.

3.1. Foster Capacitor Element Effects on the MS

The tuning behavior of the antenna under investigation in Fig. 1 is simulated for some discrete values of the Foster capacitor. Fig. 5 illustrates the variations of the MS of Mode 1 and Mode 4 with frequency. It is observed that with the capacitor tuning from 2 to 10 pF, the maximum MS of Mode 1 is shifted left. For the MS of Mode 4, the curve shows the corresponding variation around the resonant frequency of Mode 1. It implies that the resonant frequency of the ESHLA decreases with the increased capacitance. To verify this, the reflection coefficients against frequency with different values of Foster capacitor are shown in Fig. 6(a). The results show that the resonance intensity and the resonant frequency are decreased along with the increasing value of capacitor. In Fig. 6(b), the tuning susceptance vs. resonant frequency is depicted, which shows a negative slope in accordance with the expected non-Foster behavior. Therefore, by replacing the tuning Foster capacitor with an appropriate non-Foster

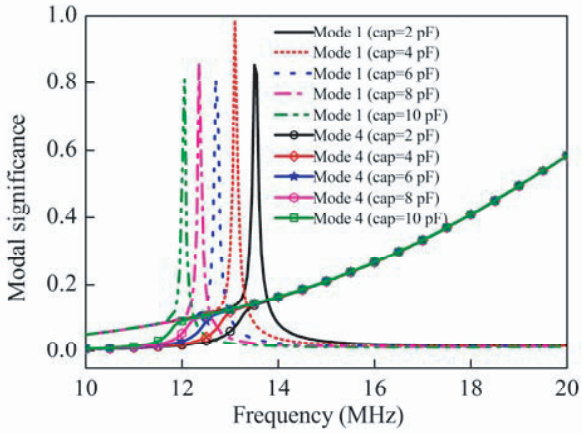

Figure 5. Modal significance of Mode 1 and Mode 4 against frequency with different values of Foster capacitor.

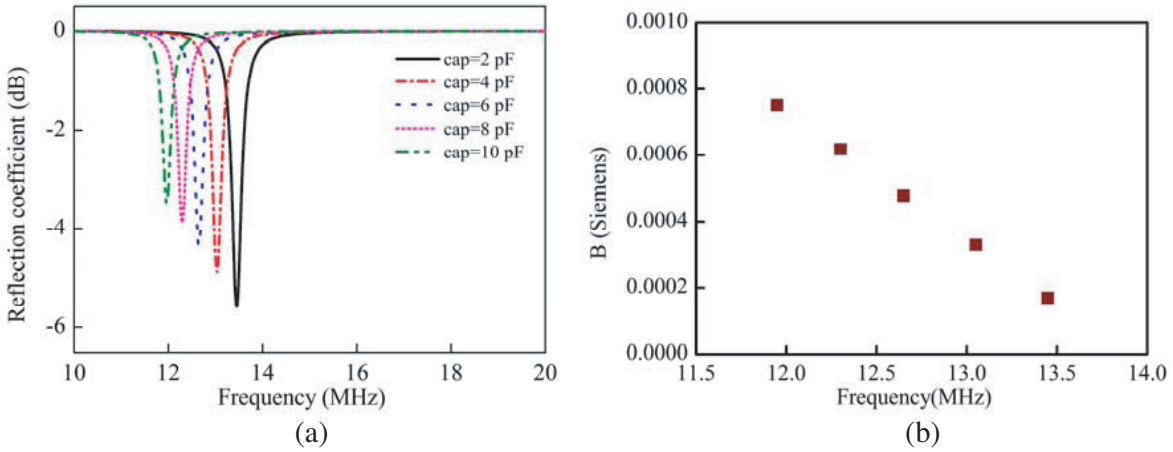

Figure 6. (a) Reflection coefficient of the Foster embedded ESHLA with different values of Foster capacitor. (b) The tuning susceptance of the Foster capacitor against resonant frequency.

network, all required tuning susceptance can be realized at once resulting in satisfying the resonance condition over a wide bandwidth.

3.2. Determination of the Non-Foster Network

Based on the parameter study above, non-Foster elements including negative capacitors and negative inductors are good choices to replace the Foster elements embedded in the ESHLA. In terms of reactance, the reactance of a negative capacitor is positive and shows negative slope with frequency, which is the opposite of the reactance of a positive capacitor. The reactance of a negative inductor is negative and shows negative slope with frequency, which is the opposite of the reactance of a positive inductor. Both negative capacitors and negative inductors produce reactance that has a negative slope with frequency. Ideally, a negative capacitor can replace some discrete inductors, whose value decreases causing an increasing resonant frequency. On the contrary, a negative inductor can replace some discrete capacitor, whose value decreases causing increasing resonant frequency. In our design, the discrete Foster capacitors can be replaced by the non-Foster network, as they show a negative slope with the resonant frequency.

To be fitted to the antenna tuning data in Fig. 6(b), a non-Foster network including a negative inductor is necessary because it can generate negative reactance that has a negative slope with frequency. However, only one negative inductor cannot closely fit to the negative slope graph over a wide bandwidth. Considering the resonant model suitable for the ESHLA (parallel model) and the type of tuning element (Foster capacitor), a negative inductor (L_{negative}) in parallel with a negative capacitor (C_{negative}) is a good choice to match the ESHLA. To find the best situation, the extracted Touchstone S-parameter file of the antenna and the embedded matching circuit are co-simulated using the Agilent Advanced Design System 2011 (ADS). By setting the goal of reflection coefficient less than -6 dB and using the random optimizer, ADS optimizes two variables, i.e., the negative inductor L_{negative} and the negative capacitor C_{negative}. Optimized results show that the non-Foster network adopts the circuit of a negative inductor in parallel with a negative capacitor, whose values are $L_{\text{negative}} = -4.16285\,\mu\text{H}$ and $C_{\text{negative}} = -37.2436\,\text{pF}$, respectively.

4. SIMULATED AND MEASURED RESULTS OF NON-FOSTER NETWORK EMBEDDED ESHLA

4.1. Simulated Results of the Non-Foster Network Embedded ESHLA

We focus on how the embedded non-Foster network affects the CMs and changes the impedance bandwidth of the ESHLA. Fig. 7 shows the MS variations with frequency for the first four modes of the antenna with the embedded non-Foster matching network. Compared to the simulated results of

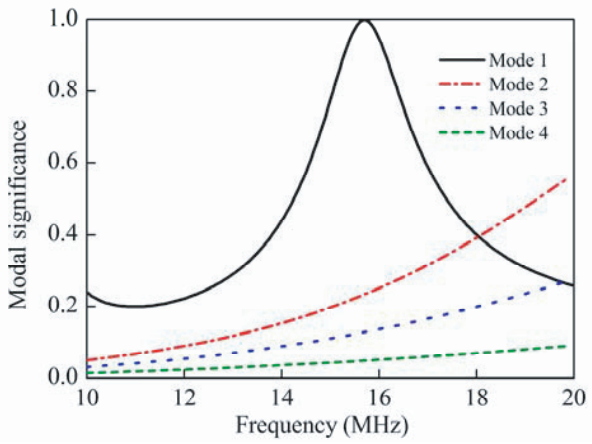

Figure 7. The simulated model significance against frequency for the non-Foster network embedded ESHLA.

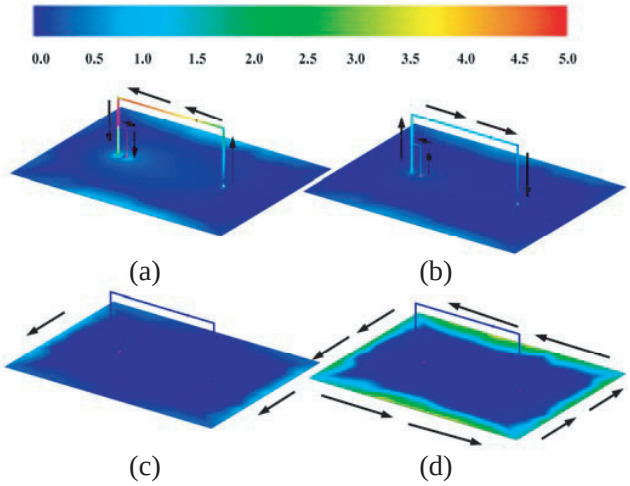

Figure 8. Characteristic currents of the first four modes at 15 MHz for the ESHLA embedded with non-Foster elements. (a) Mode 1, (b) Mode 2, (c) Mode 3, and (d) Mode 4.

the underlying passive antenna, results show that the MS curve of the modified Mode 1 becomes smooth, whose MS value is greater than 0.2 over the whole band. Thus, this modified Mode 1 breaks the narrow band restriction. The MS of the other three modes increase with frequency. Thus, the introduced non-Foster network changes the characteristic of the conventional CMs of the ESHLA. Because the modified Mode 1 breaks the narrow band restriction and resonates over a wide bandwidth, it becomes a new kind of resonant mode, i.e., a continuous resonant mode.

The characteristic currents of the first four modes for the non-Foster network embedded ESHLA at 15 MHz are shown in Fig. 8. The black arrows show the direction of the currents. The characteristic currents of the modified Mode 1 and Mode 2 flow predominantly on the half-loop, where Mode 1 resonates very strongly. Those of Mode 4 are concentrated on the edge of the finite ground. Mode 3 almost does not participate in the resonance. What's more, the flow directions on the antenna of the modified Mode 1 and Mode 2 are opposite. Thus, introducing the non-Foster network keeps parallel resonance of the antenna, but it changes the distribution and directions of the currents of the first four CMs.

To test the resonant characteristic of the modified Mode 1 over a wide band, the normalized characteristic electrical fields of Mode 1 on 13, 14, 15, and 16 MHz are shown in Fig. 9. To observe clearly, the range value of the magnitude is set from -3 to 0 dB. As can be seen, varying frequencies make only minor changes about the maximum radiating points and the radiation patterns of the characteristic electrical fields of the modified Mode 1.

Synthetically analyzing the simulated results of the non-Foster network embedded ESHLA on the MS, characteristic current distributions, and characteristic electrical fields, we can conclude that the modified Mode 1 breaks the narrow-band restriction. In the respect of characteristic field, the modified Mode 1 can also generate the desired omnidirectional radiation patterns at both horizontal and vertical planes, keeping almost the same characteristic electrical field over a quite wide band. Thus, the modified Mode 1 resonates over a wide bandwidth and becomes a continuous resonant mode. Besides, the introduced non-Foster network also alters the characteristic of the other modes.

The simulated reflection coefficient of the non-Foster embedded ESHLA is shown in Fig. 10. The 6-dB return loss bandwidth is 16.7% (from 13.7 to 16.2 MHz). It is worth mentioning that the curve of the reflection coefficient depicted in Fig. 10 is an envelope of the reflection coefficients of Foster embedded ESHLA. Thus, the non-Foster network embedded ESHLA breaks the gain-bandwidth product limitation of an electrically small antenna. The simulated gain and realized gain of the non-Foster embedded ESHLA are shown in Fig. 11, which vary slowly with frequency. The gain ranges from 1.12 to 1.19 dBi over the operating band, whereas the realized gain ranges from -0.17 to 0.56 dBi. Fig. 12 illustrates

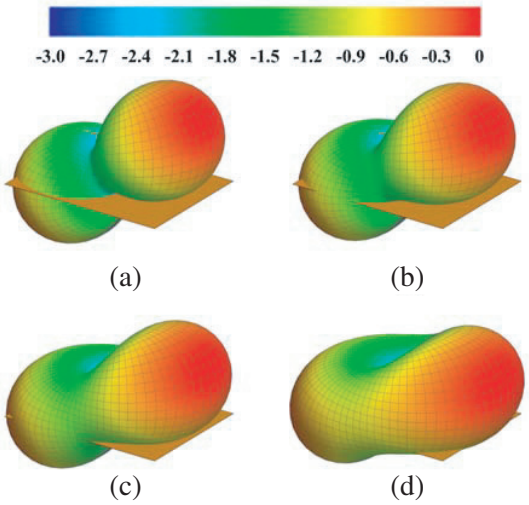

Figure 9. Normalized characteristic electrical fields of Mode 1 at different frequencies for the non-Foster network embedded ESHLA. (a) 13 MHz, (b) 14 MHz, (c) 15 MHz, and (d) 16 MHz.

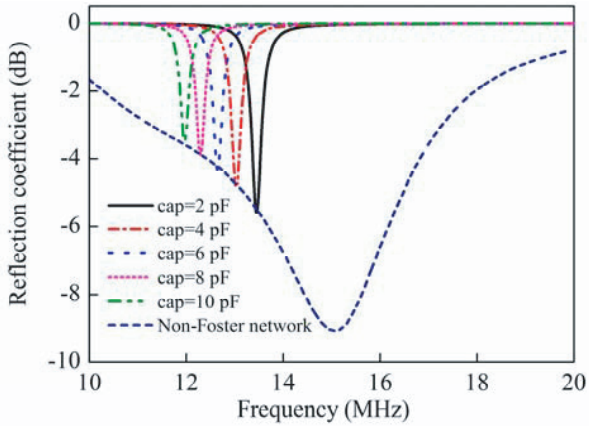

Figure 10. Simulated reflection coefficients of ESHLA embedded with a non-Foster network and Foster elements against frequency.

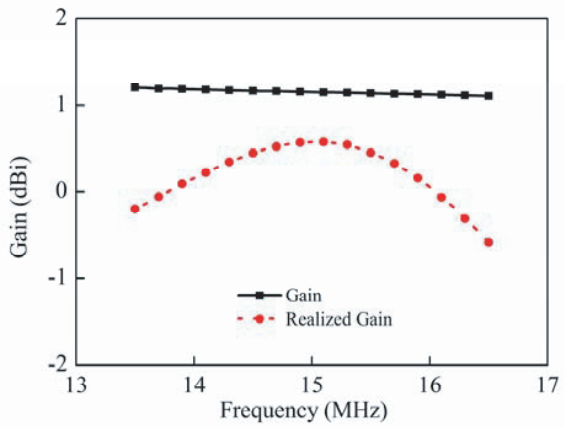

Figure 11. Simulated gains of the non-Foster network embedded ESHLA against frequency.

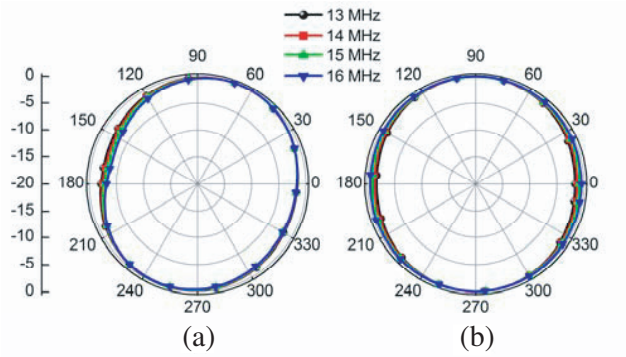

Figure 12. Simulated total radiation patterns of the non-Foster network embedded ESHLA at 13, 14, 15, and 16 MHz. (a) YOZ plane, (b) XOY plane.

the simulated normalized total radiation patterns on YOZ and XOY planes at 13, 14, 15, and 16 MHz, respectively. It can be seen that good omnidirectional performance in XOY plane is obtained, with the gain variations less than 1.3 dBi. The maximum radiating point titling 20° instead of the horizontal YOZ plane is due to the influence of the finite ground.

4.2. Measured Results of the Non-Foster Network Embedded ESHLA

The schematic of the non-Foster network embedded ESHLA, along with the dimensions, is shown in Fig. 1. The fabricated antenna is depicted in Fig. 13. The metal lines with length of 1 m surrounding the plane ground work as the extending ground plane. Thus, the equivalent total area of the ground plane is 3.6 m×4.8 m. The non-Foster network is achieved by connecting two negative impedance converter (NIC) circuits in parallel, which is hand-constructed using discrete components on RF-prototyping circuit

Figure 13. Fabricated non-Foster network embedded ESHLA.

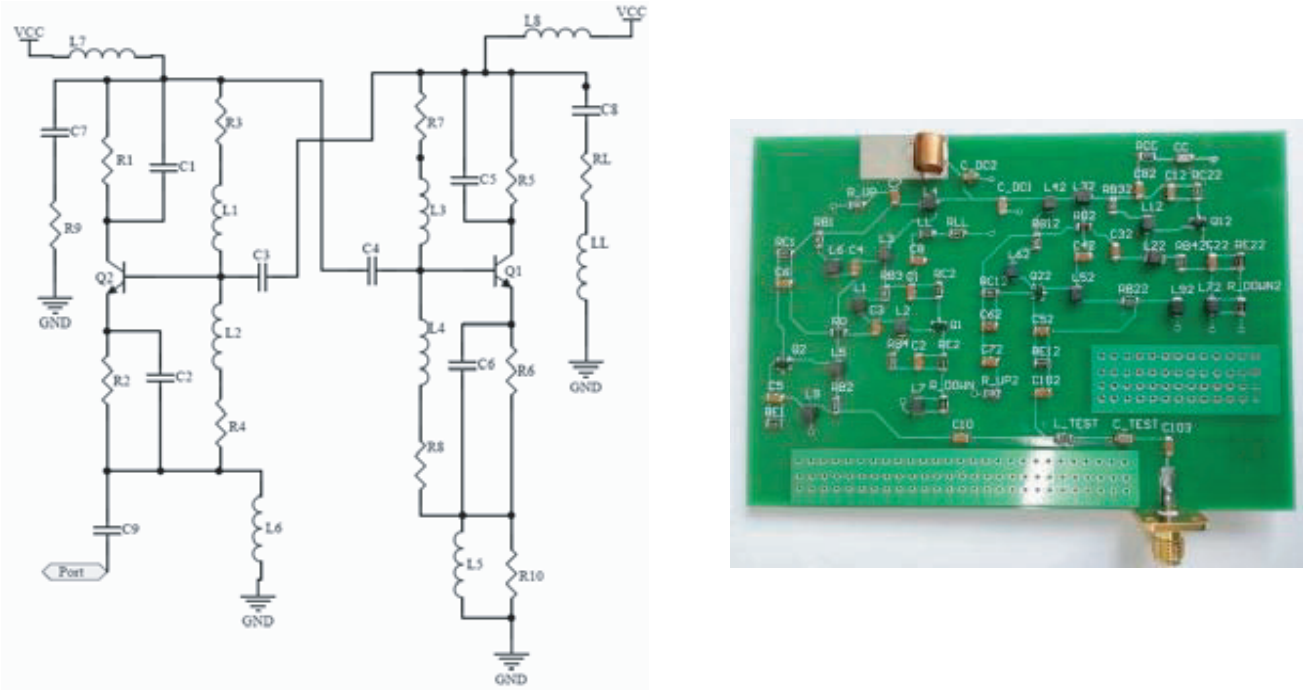

(a) (b)

Figure 14. (a) Schematic of the negative impedance converter (NIC) circuit; (b) fabricated non-Foster network.

boards with height of 1 mm. The two NIC circuits realize negative inductor and negative capacitor, respectively. The whole non-Foster network is implemented in a space equal to 15 mm × 18 mm. The output port of the non-Foster network is connected to the bottom of the pillar, whereas its ground is connected to the ground plane of the antenna.

The simulated circuit schematic of the NIC circuit for achieving a negative inductor is shown in Fig. 14(a), with its lumped element values shown in Table 2. For this design, Linvill's NIC circuit scheme [27] is used, and a detailed schematic has been presented in [28]. Thus, a proper circuit for the frequency range of HF band is designed for the proposed ESHLA. Specifically, an NPN bipolar junction transistor (BJT), BF599, is selected for our NIC circuit design. The transmission lines are not taken into account in the circuit model because of the HF band. Resistors $R9$ and $R10$ are employed to adjust the proportion of the negative converter. Inductor LL works for achieving the negative slope inductance

Table 2. Lumped element values for the proposed non-foster circuit.

Elements	Values	Elements	Values	Elements	Values	Elements	Values	Elements	Values
$R1$ (Ω)	500	$R2$ (Ω)	840	$R3$ (Ω)	75 k	$R4$ (Ω)	42k	$R5$ (Ω)	500
$R6$ (Ω)	840	$R7$ (Ω)	42k	$R8$ (Ω)	75 k	$R9$ (Ω)	150	$R10$ (Ω)	50
RL (Ω)	2.1	$C1$ (μF)	0.36	$C2$ (μF)	0.36	$C3$ (μF)	0.36	$C4$ (μF)	0.36
$C5$ (μF)	0.36	$C6$ (μF)	0.36	$C7$ (μF)	0.36	$C8$ (μF)	0.36	$C9$ (μF)	0.36
$L1$ (μH)	200	$L2$ (μH)	200	$L3$ (μH)	200	$L4$ (μH)	200	$L5$ (μH)	200
$L6$ (μH)	200	$L7$ (μH)	200	$L8$ (μH)	200	LL (μH)	2.29	VCC (V)	7.65

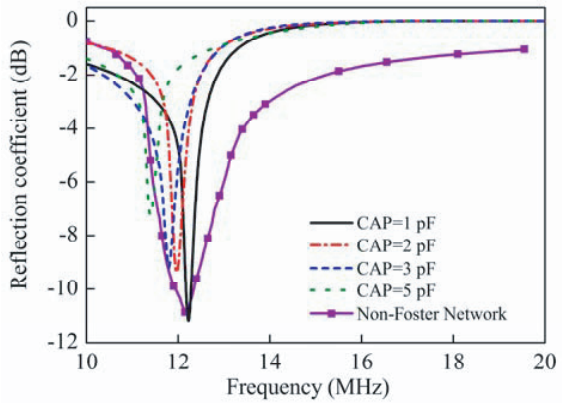

Figure 15. Measured reflection coefficients of the ESHLA embedded with a non-Foster network and Foster elements against frequency.

value. The series resistor RL is added to provide more adjustability to fit the slope. This circuit can also achieve negative capacitor when the negative conversion of inductor LL is replaced by a negative conversion of capacitor CC. Guaranteeing the same quiescent operation points of the two BJTs is the key to make the circuit work steadily. In actual fabrication of the non-Foster network, two NIC circuits are in parallel, where one provides a negative inductor, and the other provides a negative capacitor. AC lines use microstrip lines of 15 mil, and DC lines use microstrip lines of 25 mil. Two capacitors of 10 pF and 1 μF are in parallel between the power source and the ground for clutter reject, which are not shown in the circuit schematic. A resistor of 1000 Ω is crossed between the base and the collector of the coupled transistors to guarantee the stability of the quiescent operation points. A resistor and an inductor are added at the beginning of the non-Foster network port for more flexibility to adjust the impedance and a more stable circuit. The fabricated picture of the non-Foster network circuit is shown in Fig. 14(b).

Because of the stability properties, it is not possible to measure the impedance of the fabricated non-Foster network directly. Thus, we load it between the bottom of the ESHLA and the ground, and measure the reflection coefficient of the whole antenna. By adjusting the key elements to achieve negative impedance, a better result is obtained. The measured reflection coefficient results of the ESHLA with the embedded original Foster element and the non-Foster matching network are shown in Fig. 15. As can be seen, the resonance intensity and resonant frequency are decreased along with the increasing value of the capacitor. Owing to the machining precision and tolerance, the resonant frequency is offset. The measured reflection coefficient of the ESHLA embedded with non-Foster elements shows that the relative bandwidth below −6 dB is 12.7% (from 11.45 to 13 MHz), which is more than six times greater than the measured reflection coefficients of the underlying passive ESHLA.

5. CONCLUSION

An ESHLA is investigated in this paper. The antenna size is $0.05\lambda \times 0.025\lambda$ (λ is the free-space wavelength at 15 MHz). With Foster elements embedded in it, the ESHLA resonates weakly at 13.45 MHz, which shows fairly narrow bandwidth at HF band. Based on the basis analysis of CM theory, it is found that Mode 1 is the resonant mode, and the antenna resonates at parallel resonance. Parameter analysis shows that tuning Foster capacitor leads to a variation of resonant frequency, generating a negative slope between admittance and the resonant frequency in accordance with the expected Non-Foster behavior. Thus, a non-Foster network is embedded replacing the Foster capacitor. Results show that the non-Foster network not only alters the characteristics of the other higher order modes but also changes the modified Mode 1 from narrowband resonant mode into a new mode, i.e., a continuous resonant mode. What's more, the radiation pattern of the continuous resonant mode is stable, leading to a stable radiation pattern and gain of the proposed antenna over the whole operating band. The simulated and measured 6-dB return loss bandwidths are 16.7% (from 13.7 to 16.2 MHz) and 12.7% (from 11.45 to 13 MHz), respectively. In addition, the characteristic of omnidirectional radiation pattern shows that ESHLA embedded with the non-Foster network can be a good candidate for the use in mobile communication in HF band.

ACKNOWLEDGMENT

This work is supported by National Natural Science Foundation of China (No. 61372002 Broadband and Miniaturized Antenna Using Non-Foster Reactance Circuits).

REFERENCES

1. Wei, T. and H. L. Zheng, "An optimised of high-efficiency vehicular loop antenna for NVIS applications," *2010 International Conference on Microwave and Millimeter Wave Technology (ICMMT)*, 1252–1255, May 8–11, 2010.
2. Austin, B. and K. Murray, "The application of characteristic-mode techniques to vehicle-mounted NVIS antennas," *IEEE Antennas Propag. Mag.*, Vol. 40, No. 1, 7–21, Feb. 30, 1998.
3. Zhou, G. P. and G. S. Smith, "An accurate theoretical model for the thin-wire circular half-loop antenna," *IEEE Trans. Antennas Propagat.*, Vol. 39, No. 8, 1167–1177, Aug. 1991.
4. Packer, M. J. and P. A. Diez, "Electrically small half-loop antenna analysis by numerical emulation," *Proc. 10th IET International Conference on IRST, 2006*, 64–68, Jul. 18–21, 2006.
5. Zhou, G. P. and G. S. Smith, "The multiturn half-loop antenna," *IEEE Trans. Antennas Propagat.*, Vol. 42, No. 5, 750–754, May 1994.
6. Liu, H. T., Y. H. Cheng, and M. Yan, "Electrically small loop antenna standing on compact ground in wireless sensor package," *IEEE Antennas Wireless Propag. Lett.*, Vol. 15, No. 99, 1-1, 2015.
7. Koubeissi, M., B. Pomie, and E. Rochefort, "Perspectives of HF half loop antennas for stealth combat ships," *Progress In Electromagnetics Research B*, Vol. 54, 167–184, 2013.
8. Gouin, J. P., D. Lafargue, and H. L. Guen, "HF 125 W half-loop antennas in ALE and ECCM for land mobile, navy and helicopter use," *Proc. Eighth International conference on HF Radio Systems and Techniques*, 49–52, 2000.
9. Chu, L. J., "Physical limitations of omni-directional antennas," *Journal of Applied Physics*, Vol. 19, 1163–1175, Dec. 1948.
10. Wheeler, H. A., "Fundamental limitations of small antennas," *Proc. IRE*, Vol. 35, No. 12, 1479–1484, Dec. 1947.
11. Ouedraogo, R. O., E. J. Rothwell, A. Diaz, S.-Y. Chen, A. Temme, and K. Fuchi, "In situ optimization of metamaterial-inspired loop antennas," *IEEE Antenna Wireless Propag. Lett.*, Vol. 9, 75–78, 2010.

12. Ramanandraibe, E., M. Latrach, W. Abdouni, and A. Sharaiha, "A half-loop antenna associated with one SRR cell," *Proc. 2013 International Conference on Electromagnetics in Advanced Applications (ICEAA)*, 1442–1445, 2013.
13. Ramanandraibe, E., M. Latrach, and A. Sharaiha, "Multi-band metamaterial-inspired half-loop antenna," *Proc. 2014 International Conference on Multimedia Computing and Systems (ICMCS)*, 1449–1452, 2014.
14. Mirzaei, H. and G. V. Eleftheriades, "A resonant printed monopole antenna with an embedded non-foster matching network," *IEEE Trans. Antennas Propagat.*, Vol. 61, No. 11, 5363–5371, Nov. 2013.
15. Barbuto, M., A. Monti, F. Bilotti, and A. Toscano, "Design of a non-foster actively loaded SRR and application in metamaterial-inspired components," *IEEE Trans. Antennas Propagat.*, Vol. 61, No. 3, 1219–1227, Mar. 2013.
16. Church, J., J.-C. S. Chieh, L. Xu, J. D. Rockway, and D. Arceo, "UHF electrically small box cage loop antenna with an embedded non-foster load," *IEEE Antenna Wireless Propag. Lett.*, Vol. 13, 1329–1332, 2014.
17. Fan, Y. F., K. Z. Rajab, M. Munoz, and Y. Hao, "Electrically small half-loop antenna design with non-Foster matching networks," *Proc. 6th European Conference on Antennas and Propagation (EUCAP)*, 126–129, 2011.
18. Albarracín-Vargas, F., E. Ugarte-Muñoz, V. González-Posadas, and D. Segovia-Vargas, "Sensitivity analysis for active matched antennas with non-Foster elements," *IEEE Trans. Antennas Propagat.*, Vol. 62, No. 12, 6040–6048, Dec. 2014.
19. Garbacz, R. J. and R. Turpin, "A generalized expansion for radiated and scattered fields," *IEEE Trans. Antennas Propagat.*, Vol. 19, No. 3, 348–358, May 1971.
20. Harrington, R. F. and J. R. Mautz, "Theory of characteristic modes for conducting bodies," *IEEE Trans. Antennas Propagat.*, Vol. 19, No. 5, 622–628, Sep. 1971.
21. Harrington, R. F. and J. R. Mautz, "Computation of characteristic modes for conducting bodies," *IEEE Trans. Antennas Propagat.*, Vol. 19, No. 5, 629–639, Sep. 1971.
22. Garbacz, R. J. and D. M. Pozar, "Antenna shape synthesis using characteristic modes," *IEEE Trans. Antennas Propagat.*, Vol. 30, No. 3, 340–350, May 1982.
23. Liu, D., R. J. Garbacz, and D. M. Pozar, "Antenna synthesis and optimization using generalized characteristic modes," *IEEE Trans. Antennas Propagat.*, Vol. 38, No. 6, 62–868, Jun. 1990.
24. Harrington, R. F. and J. R. Mautz, "Control of radar scattering by reactive loading," *IEEE Trans. Antennas Propagat.*, Vol. 20, No. 4, 446–454, Jul. 1972.
25. Adams, J. J. and J. T. Bernhard, "A modal approach to tuning and bandwidth enhancement of an electrically small antenna," *IEEE Trans. Antennas Propagat.*, Vol. 59, No. 4, 1085–1092, Apr. 2011.
26. Obeidat, K. A., B. D. Raines, and R. G. Rojas, "Discussion of series and parallel resonance phenomena in the input impedance of antennas," *Radio Sci.*, Vol. 45, No. 6, RS6012, Dec. 2010.
27. Linvill, J., "Transistor negative-impedance converters," *Proc. IRE*, Vol. 41, No. 6, 725–729, Jun. 1953.
28. Jacob, M. M., L. Jiang, and D. F. Sievenpiper, "Non-Foster loaded parasitic array for broadband steerable patterns," *IEEE Trans. Antennas Propagat.*, Vol. 62, No. 12, 6081–6090, Dec. 2014.